AIAA JOURNAL
Vol. 49, No. 11, November 2011

Technical Notes

Extension and Exploration of a Hybrid Turbulence Model on Unstructured Grids

C. Eric Lynch* and Marilyn J. Smith†
Georgia Institute of Technology, Atlanta, Georgia 30332-0150

DOI: 10.2514/1.J051177

I. Introduction

MOST fluid flows of engineering interest are turbulent, and while numerous advances have been made in the numerical solution of the Navier–Stokes equations, known as computational fluid dynamics (CFD), turbulent flows still present challenges for today's methods. Turbulent flows are characterized by a very wide range of scales in both time and space. Most of the kinetic energy of a turbulent flow is stored in the large-scale structures of the flow. In contrast, kinetic energy is dissipated as heat at the smallest scales. Although the much more computationally intensive large eddy simulations (LES) and direct numerical simulations (DNS) are performed in research environments, simulations that resolve the Reynolds-averaged Navier–Stokes (RANS) equations are still required for rapid engineering results. The size of the smallest length scales, and therefore the maximum allowable CFD grid spacing to completely resolve all turbulence, is inversely proportional to $Re^{3/4}$. So for a three-dimensional simulation, the number of grid points must scale with $Re^{9/4}$ [1]. Because such fine grids and small time steps are not practical with today's computers, compromises must be made that approximate certain aspects of the physics.

Most CFD methods solve the steady or unsteady RANS (URANS) equations, as illustrated in Fig. 1. Essentially, only the mean flow is solved on the computational mesh, and the turbulent physics are replaced by *closure* models of varying sophistication. URANS–based methods include simple algebraic models like Baldwin–Lomax, one-equation models like Baldwin–Barth and Spalart–Allmaras, and two-equation models such as k-ω and k-ω shear stress transport (SST). These turbulence models tend to be heuristic and rely on nonphysical constants that are "tuned" to specific flows, such as airfoils at low angles of attack. That is, the results from the model are iteratively compared against experimental data, and the constants are adjusted until the computational results agree with the experiment. Although they perform well for those cases, they fail to accurately predict unsteady flows dominated by viscous effects, as in the case of static and dynamic stall [2,3] or bluff-body flows.

Hybrid RANS/LES methods provide a way to achieve some of the advantages of LES for separated and highly vortical flowfields while retaining the computational efficiency of URANS methods. Baurle et al. [4] developed the idea that URANS and LES methods can be linearly blended by some smooth function to form a hybrid model. This idea of blending was used in 2006 by Sanchez-Rocha et al. [5], who used the k-ω SST RANS model as the basis for a hybrid method within an existing LES code to resolve wall-bounded turbulence. Sanchez-Rocha et al. demonstrated this capability with simulations of a NACA 0015 airfoil in static and dynamic stall at a Reynolds number of 1×10^6. A more common approach is to incorporate an LES model into a URANS code to capture subgrid scales, so that where grid resolution permits, LES-like results are obtained. Strictly speaking, LES requires that the resolved scales extend into the inertial subrange. These scales, and those smaller, are more *universal*, meaning that their physics depends less on the particular geometry. Such universal scales are more amenable to modeling, since even when heuristics are used, they should be valid for a larger range of flows. The drawback of LES is that in order to directly solve for the larger turbulent scales, it requires much finer grids and smaller time steps than URANS computations. In most engineering applications, LES remains far too computationally expensive for routine use. On coarse grids that are usually only suitable for URANS applications, hybrid methods of this variety can capture larger turbulent eddies in the interior of the flow (away from boundaries), thus providing a better approximation of the true physics than URANS alone.

Detached eddy simulation (DES) is a common hybrid formulation, in which the turbulence near walls is modeled with Menter's k-ω SST [6] or Spalart–Allmaras [7] URANS turbulence models. However, it must be noted that DES models are separate and distinct from hybrid methods like those of Sanchez-Rocha et al. [5] in that they lack a dedicated subgrid-scale model. Instead, the URANS equations perform "double-duty" as the LES model by modifying a length scale used in the destruction terms [8,9].

For this effort, the RANS–LES hybrid model developed by Sanchez-Rocha et al. [5,10] has been extended and evaluated within an unstructured CFD methodology. Comparisons with experimental data, as well as published LES and structured CFD simulations, were used to verify and expand the base of knowledge of unstructured hybrid RANS–LES methods. Emphasis is placed on the improvement of the aerodynamic performance quantities (forces and moments) through more accurate prediction of the pressure distribution and separation location on the cylinder.

II. Method Verification

The hybrid RANS–LES model has been extended to include unstructured topologies and implemented into NASA Langley's unstructured CFD solver FUN3D. FUN3D implicitly solves the URANS equations using node-centered, unstructured, mixed-element meshes [11–13], and has been successfully used for a number of applications that encompass the aerospace spectrum [14–16]. Time-accurate solutions use a second-order backward differentiation formula. The resulting linear system of equations is solved using a point-implicit relaxation scheme.

The hybrid RANS–LES method (HR-LES) was evaluated with a circular cylinder at a Mach number of 0.2 and a diameter-based Reynolds number of 3900 at standard sea-level conditions on three different grid systems. These evaluations use fully unstructured grids that were generated as a two-dimensional mesh of triangle elements and quadrilateral elements (the latter in the boundary layer) and then extruded in the spanwise direction to form prismatic elements. This strategy permits a straightforward variation of the spanwise resolution, which has been demonstrated [17] to be an important factor in accurate CFD solutions of separated flows. The first grid had

Presented at the 38th Fluid Dynamics Conference and Exhibit, Seattle, WA, 23–26 June 2008; received 17 January 2011; revision received 4 May 2011; accepted for publication 30 May 2011.

*Ph.D. Candidate, School of Aerospace Engineering. Student Member AIAA.

†Associate Professor, School of Aerospace Engineering. Associate Fellow AIAA.

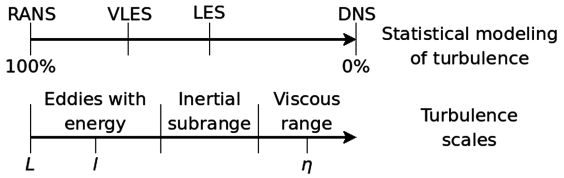

Fig. 1 Illustration of the resolution of turbulence scales by numerical techniques.

51 planes spaced evenly over a four-diameter span, the second had 101 planes over four diameters, and the third had 101 planes over eight diameters, yielding the same number of nodes as the second grid, but with larger cell aspect ratios. A radial cross section of the grid contains 123,652 nodes, 203,492 triangular elements, and 21,363 quadrilateral elements. Normal spacing was such that $y^+ \ll 1$. A refined nondimensional time step of $\Delta t a_\infty / D = 0.025$ provided approximately 1000 time steps per vortex shedding cycle.

Figure 2 presents isosurfaces of the vortex-identification criterion [18], sometimes called *Q criterion*, for the three-dimensional cylinder at $Re = 3900$ on the three grids. The definition of Q is such that it is only positive near vortices. In flow visualizations, this property can be used to filter out the "sheets" of high vorticity that emanate from turbulent boundary layers, revealing vortices. Although the k-ω SST model captures periodic vortex shedding in three dimensions, whereas it did not in two dimensions, those vortices are essentially two-dimensional across the span (Fig. 2a). In contrast, the hybrid RANS–LES results on all grids show substantial spanwise variation and a much more irregular wake (Fig. 2b–2d). Since k-ω SST yields a result that could have been obtained on a substantially reduced grid (or whatever the method requires for a two-dimensional simulation), the majority of the grid nodes have simply added to the overall cost of the computation.

Table 1 delineates the various statistics for the cylinder predictions, including mean drag coefficient, Strouhal number, and separation location. Strouhal number is calculated from the frequency spectrum of the fluctuating lift. Separation location is given in degrees over the circumference of the cylinder from the leading-edge stagnation point to the point where skin friction along the cylinder centerline drops to zero. All three-dimensional cases predict the Strouhal number within experimental bounds, regardless of turbulence model. However, the three-dimensional k-ω SST simulation yields a drag coefficient over 1.4, close to the result of a two-dimensional hybrid RANS–LES simulation. With three-dimensional hybrid RANS–LES, drag is predicted much closer to the experimental value, though it is still slightly underpredicted on all grids. All

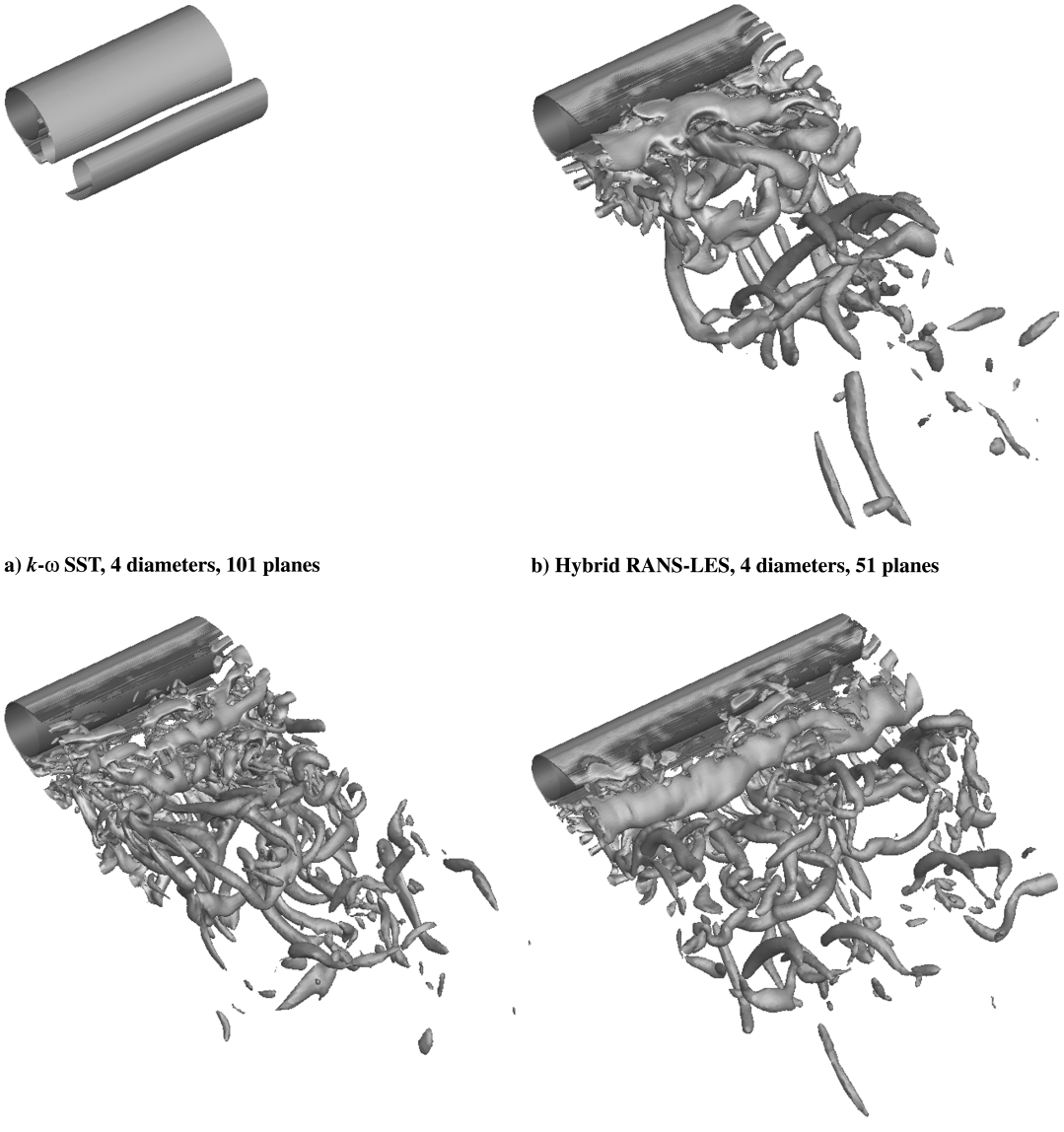

a) k-ω SST, 4 diameters, 101 planes

b) Hybrid RANS-LES, 4 diameters, 51 planes

c) Hybrid RANS-LES, 4 diameters, 101 planes

d) Hybrid RANS-LES, 8 diameters, 101 planes

Fig. 2 Isosurfaces of Q criterion about a three-dimensional circular cylinder with varying grid resolution.

Table 1 Predicted characteristics for various turbulence methods and grids

N_z	Z	Turbulence model	Mean C_D	Strouhal no.	Separation location[a]
——	——	Experiment	0.99 ± 0.05	0.215 ± 0.005 [19]	$86 \pm 2°$ [20]
101	$4D$	k-ω SST	1.456	0.213	98.4°
2	——	HR-DES	1.5	0.25	86.8°
51	$4D$	HR-LES	0.971	0.216	85.8°
101	$4D$	HR-LES	0.919	0.217	84.3°
101	$8D$	HR-LES	0.939	0.217	84.7°
48	πD	LES [21]	1.04	0.210	88.0°

[a]Separation location is given in degrees of azimuth from the leading-edge stagnation point.

hybrid RANS–LES simulations predict the separation location within the experimental bounds, while k-ω SST predicts it over 10° farther aft.

Figure 3 shows mean pressure coefficient along the cylinder centerline, from the leading-edge stagnation point ($\theta = 0$) to 180° opposite. There, it is clear that the hybrid RANS–LES simulations better predict drag because they do not overpredict base suction to the extent that the k-ω SST simulation does. Figure 4 shows the correlation between computed and measured centerline C_p, with any points on a diagonal line with a 45° slope being in perfect agreement with the measured data. The zoomed in region in Fig. 4b indicates that the grid with a diameter of $4D$ and 51 spanwise planes has the best correlation once the flow is separated.

Unlike their structured grid counterparts, which only allow hexahedral cells, unstructured CFD solvers may allow a variety of cell types. In structured formulations, very high cell aspect ratios are quite common in directions where flow gradients are expected to be small. However, in unstructured frameworks, tetrahedral cells of very high aspect ratio, which are commonly seen in boundary layers, pose special problems. Figures 5a and 5b depict isosurfaces of vorticity magnitude on the three-dimensional cylinder using tetrahedral and prismatic boundary-layer cells. The tetrahedral boundary-layer solution indicates the presence of numerical errors in the form of spurious vorticity upstream of the leading edge. These errors are not present when the boundary layer is modeled with prismatic cells.

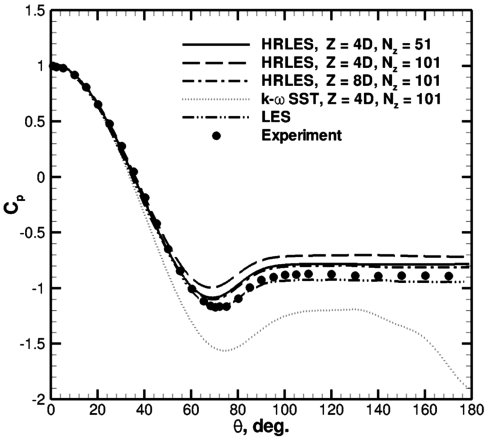

Fig. 3 Mean pressure coefficient along the centerline for the three-dimensional circular cylinder on several grids with varying turbulence methods. LES data are from [21], and experimental data are digitized from Fig. 11 in [21].

Node-centered solvers typically use an edge-based scheme in which fluxes are evaluated along the edges of the primal grid. Since each primal edge corresponds to a face in the dual mesh, this is approximately equivalent to evaluating fluxes across the dual faces. In highly stretched tetrahedral cells, some dual faces and primal edges will be nearly parallel, yielding a very poor approximation of gradients across those faces, which exacerbates the dispersion-dissipation errors that are inherent in unstructured methods, in particular at near-zero velocities at the stagnation pressure location. In turn, this reduces the accuracy of the reconstruction scheme, and errors propagate through the solution. Therefore, when applying this hybrid RANS–LES model, care should be taken to use prismatic cells in the boundary layer.

Profiles of the streamwise velocity u/U_∞ at seven downstream wake traverse locations on the mesh with 101 planes over four diameters are shown in Fig. 6. These profiles have been averaged in time and in space, in the spanwise direction. Experimental data digitized from Figs. 13, 15, and 22 in [21], as well as LES data of Kravchenko and Moin [21], are also included. In the far wake, hybrid RANS–LES slightly overpredicts the velocity deficit, but captures the spreading of the wake observed in the experimental data. At the position closest to the wall, at $x/D = 0.58$, hybrid RANS–LES predicts the correct troughlike profile. At the first position in the recirculation region, $x/D = 1.06$, hybrid RANS–LES predicts a velocity profile that looks similar to those closer to the cylinder, continuing to produce a relatively thin shear layer. In general, in the recirculation region, the hybrid RANS–LES profile "lags" in space behind the experimental and LES data, with the profile spreading farther downstream. From Table 1, it is clear that these discrepancies in the wake do not lead to large errors in drag or shedding frequency.

The errors in Fig. 6 can be attributed in some part to grid topology. As described earlier, the mesh was originally generated in two dimensions and then extruded in the spanwise direction, which

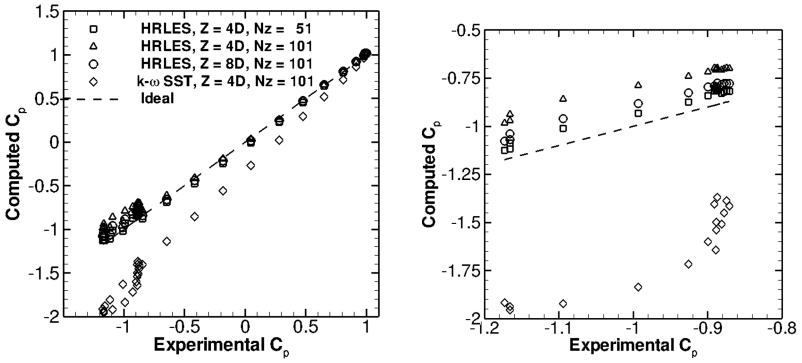

a) All data points **b) Points with $\theta > 70°$**

Fig. 4 Correlation of computed mean pressure coefficient with measured value.

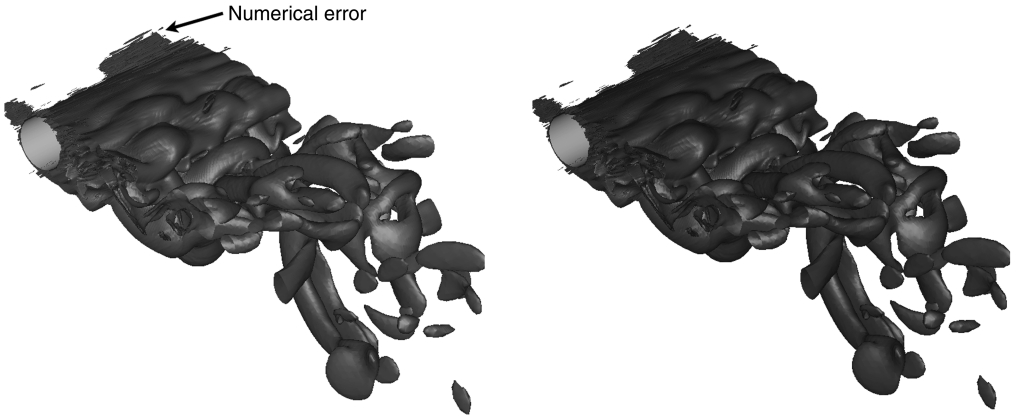

a) Tetrahedral boundary-layer cells b) Prismatic boundary-layer cells

Fig. 5 Isovorticity contours around a three-dimensional cylinder, computed using the hybrid RANS–LES model on grids with different cell types in the boundary layer.

results in cells that have aspect ratios as high as 6 in the wake outside the boundary layer and as high as 40 in the far field. The hybrid RANS–LES destruction term uses (cell volume)$^{1/3}$ as a measure of the local length scale, which implicitly assumes a nearly isotropic grid. This topology consideration is distinct from the earlier discussion of boundary-layer cell type in that the issue is not one of gradient reconstruction, but rather one of reasonably estimating the length scale representing the largest eddy that can be resolved on the grid.

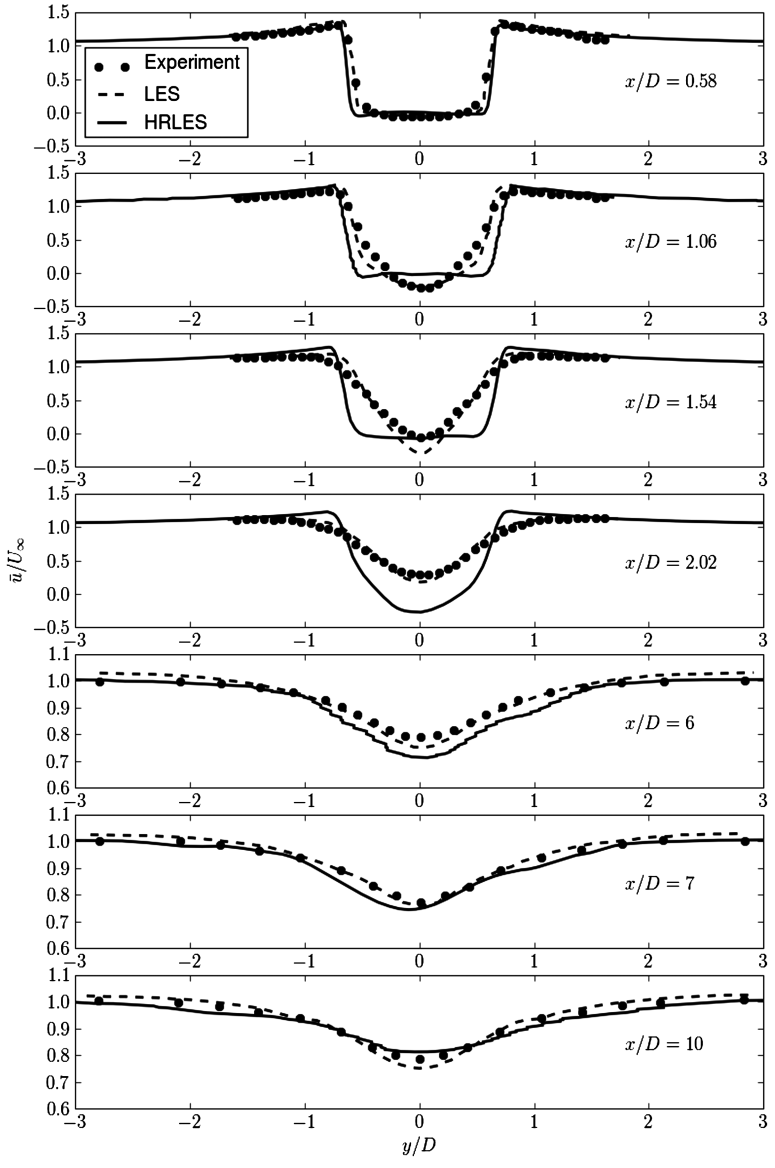

Fig. 6 Seven locations of u/U_∞ in the wake of a cylinder at $Re = 3900$ using a spanwise extruded grid.

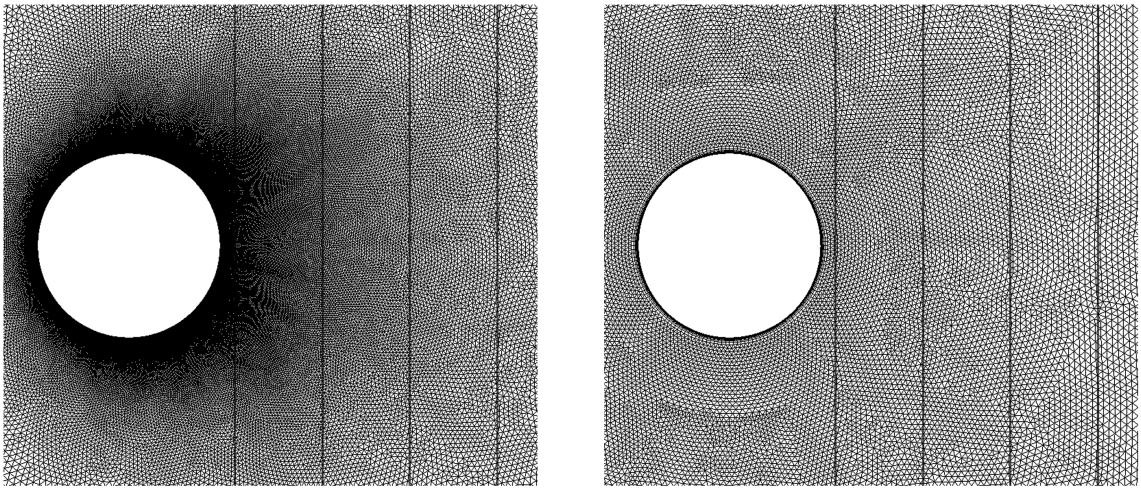

a) Extruded mesh, 101 spanwise planes over 4 diameters b) Non-extruded three-dimensional mesh

Fig. 7 Spanwise slices of the original mesh and the three-dimensional mesh used to evaluate the effect of cell stretching. Lines indicate wake traverse locations.

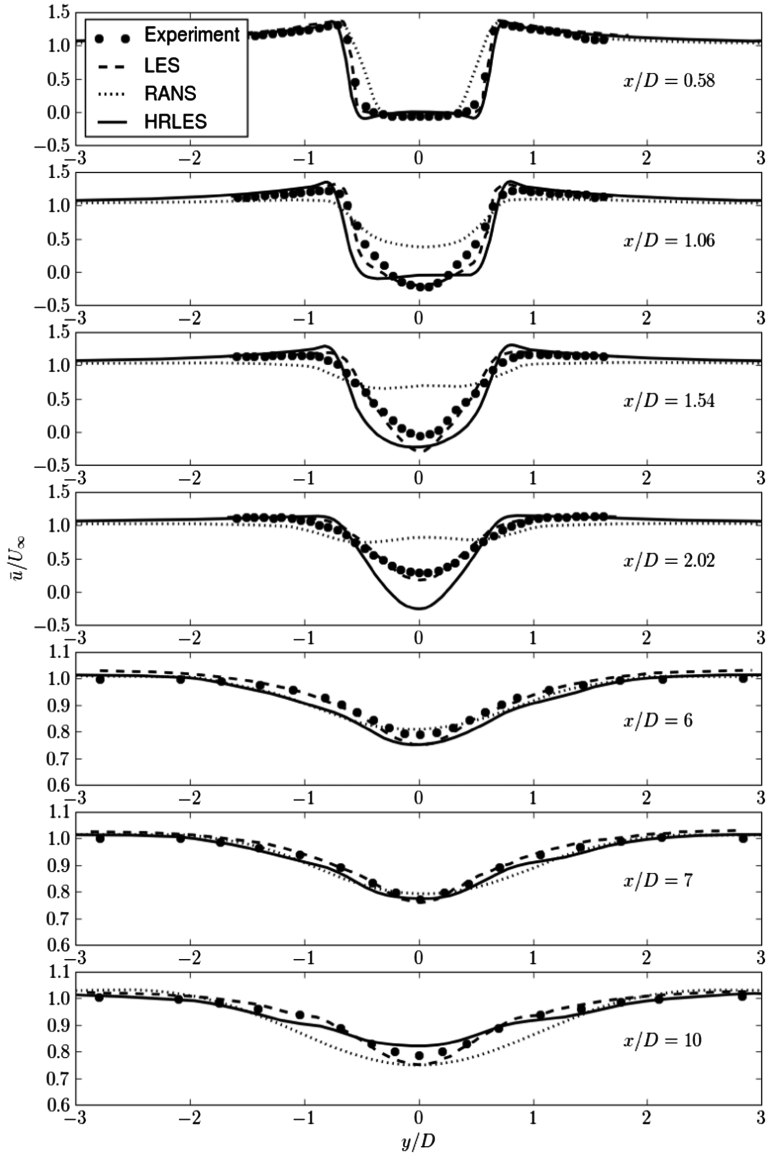

Fig. 8 Seven locations of u/U_∞ in the wake of a cylinder at $Re = 3900$ using a nonextruded three-dimensional grid.

To test the effect of grid topology, a naturally-developing three-dimensional grid was created. Instead of a defined number of spanwise points, the cells were allowed to expand in the spanwise direction at the same rate as the other two directions. Several volume mesh refinements were evaluated to ensure that the turbulent content within the separated zone aft of the cylinder was captured. The surface resolution was similar to the original mesh, but even with the volume mesh refinements the total node count that resulted in a more efficient 5 million node grid. Figure 7 shows a spanwise slice of the two grids near the four upstream traverses. Wake velocity profiles at the seven traverses are shown again in Fig. 8. The $x/D = 1.54$ and 2.02 locations show substantial improvement over the URANS predictions, with the former attaining more of the expected V-shaped profile, though still spreading more slowly than expected. Subtle improvements are visible at other traverse locations as well.

Kravchenko and Moin [21] note that this case is very sensitive to disturbances such as the freestream turbulence level. They do not specify the freestream turbulence intensity in their LES simulations, but in the present hybrid RANS–LES simulations, it was set at $\sqrt{k}/U_\infty = 4.7 \times 10^{-4}$, which may be lower than the turbulence level in the experimental results used for correlation.

Sanchez-Rocha [10] found that using constant coefficients (as is implemented here) could lead to artificial turbulence dissipation. If the wake turbulence is dissipated, there is less mixing across shear layers, possibly leading to the abrupt, square velocity profile seen at $x/D = 1.54$ in Fig. 6. These results may be improved using a fully dynamic implementation in which the coefficients are varied based on the local flow characteristics [10].

III. Conclusions

A hybrid Reynolds-averaged Navier–Stokes (RANS) and large eddy simulation (LES) turbulence model has been implemented and demonstrated in an unstructured legacy URANS computational fluid dynamics code. The hybrid method consists of a blending of the k-ω SST RANS model with a one-equation LES model for the subgrid-scale turbulence kinetic energy (k^{sgs}). The model has been demonstrated for unsteady separated flows over a static cylinder.

1) The hybrid RANS–LES method yields improved predictions of drag and shedding frequency for bluff-body flow when compared with its underlying two-equation URANS model.

2) These methods correctly predict the unsteady, 3-D, and chaotic nature of the wake.

3) The hybrid RANS–LES method examined here is sensitive to mesh cells with a very high aspect ratio.

4) Nonphysical solutions were observed for meshes containing tetrahedra with spanwise aspect ratios greater than 8 close to the wall, but outside the boundary layer. Most unstructured grid generators automatically generate low aspect ratio cells outside the boundary layer (they are unavoidable *in* the boundary layer), but in the special case of extruded meshes, special care should be taken in determining the spanwise aspect ratios to minimize the dispersion errors inherent within unstructured methods.

Acknowledgments

This material is based upon work supported by the National Science Foundation under grant no. 0731034, "Advancing Wind Turbine Analysis and Design for Sustainable Energy." This research was supported in part by the National Science Foundation through TeraGrid resources provided by The Texas Advanced Computing Center (TACC). Any opinions, findings, and conclusions or recommendations expressed in this material are those of the author(s) and do not necessarily reflect the views of the National Science Foundation. The authors would like to thank the FUN3D Development Team for their aid and discussions in this endeavor.

References

[1] Davidson, P. A., *Turbulence: An Introduction for Scientists and Engineers*, Oxford Univ. Press, New York, 2004.

[2] Smith, M. J., Potsdam, M., Wong, T.-C., Baeder, T.-C., and Phanse, S., "Evaluation of Computational Fluid Dynamics to Determine Two-Dimensional Airfoil Characteristics for Rotorcraft Applications," *Journal of the American Helicopter Society*, Vol. 51, No. 1, 2006, pp 70–79.
doi:10.4050/1.3092879

[3] Szydlowski, J., and Costes, M., "Simulation of Flow Around a NACA 0015 Airfoil for Static and Dynamic Stall Configurations Using RANS and DES," *AHS International 4th Decennial Specialists' Conference on Aeromechanics*, San Francisco, Jan. 21–23 2004.

[4] Baurle, R. A., Tam, C. J., Edwards, J. R., and Hassan, H. A., "Hybrid Simulation Approach for Cavity Flows: Blending Algorithm, and Boundary Treatment Issues," *AIAA Journal*, Vol. 41, No. 8, 2003, pp. 1463–1480.
doi:10.2514/2.2129

[5] Sanchez-Rocha, M., Kirtas, M., and Menon, S., "Zonal Hybrid RANS–LES Method for Static and Oscillating Airfoils and Wings," 44th AIAA Aerospace Sciences Meeting and Exhibit, Reno, NV, AIAA Paper 2006-1256, Jan. 9–12 2006.

[6] Menter, F. R., "Improved Two-Equation k-ω Turbulence Models for Aerodynamic Flows," NASA TM 103975, Oct. 1992.

[7] Spalart, P., and Allmaras, S., "A One-Equation Turbulence Model for Aerodynamic Flows," 30th AIAA Aerospace Sciences Meeting and Exhibit, Reno, NV, AIAA Paper 1992-0439, Jan. 6–9 1992.

[8] Travin, A., Shur, M., Strelets, M., and Spalart, P. R., "Detached-Eddy Simulation Past a Circular Cylinder," *Flow, Turbulence and Combustion*, Vol. 63, Nos. 1–4, 1999, pp. 293–313.
doi:10.1023/A:1009901401183

[9] Strelets, M., "Detached Eddy Simulation of Massively Separated Flows," 39th AIAA Aerospace Sciences Meeting and Exhibit, Reno, NV, AIAA Paper 2001-0879, Jan. 8-11 2001.

[10] Sanchez-Rocha, M., "Wall-Models for Large Eddy Simulation Based on a Generic Additive-Filter Formulation," Ph.D. Thesis, Georgia Inst. of Technology, Atlanta, 2008.

[11] Bonhaus, D., "An Upwind Multigrid Method for Solving Viscous Flows on Unstructured Triangular Meshes," M.S. Thesis, George Washington Univ., Washington, D.C., 1993.

[12] Anderson, W., and Bonhaus, D., "An Implicit Upwind Algorithm for Computing Turbulent Flows on Unstructured Grids," *Computers and Fluids*, Vol. 23, No. 1, 1994, pp. 1–21.
doi:10.1016/0045-7930(94)90023-X

[13] Anderson, W., Rausch, R., and Bonhaus, D., "Implicit/Multigrid Algorithms for Incompressible Turbulent Flows on Unstructured Grids," *Journal of Computational Physics*, Vol. 128, No. 2, 1996, pp. 391–408.
doi:10.1006/jcph.1996.0219

[14] OBrien, D. M., and Smith, M. J., "Analysis of Rotor-Fuselage Interactions Using Various Rotor Models," AIAA 43rd Aerospace Sciences Meeting, Reno, NV, AIAA Paper 2005-0468, Jan. 10–13 2005.

[15] O'Brien, D. M. J., "Analysis of Computational Modeling Techniques for Complete Rotorcraft Configurations," Ph.D. Thesis, Georgia Inst. of Technology, Atlanta, 2006.

[16] Lee-Rausch, E. M., Frink, N. T., Mavriplis, D. J., Rausch, R. D., Milholen, W. E., "Transonic Drag Prediction on a DLR-F6 Transport Configuration Using Unstructured Grid Solvers," 42nd AIAA Aerospace Sciences Meeting, Reno, NV, AIAA Paper 2004-0554, Jan. 5–8 2004.

[17] Smith, M. J., Koukol, B. C. G., Quackenbush, T., and Wachspress, D., "Reverse- and Cross-Flow Aerodynamics for High-Advance Ratio Flight," *35th European Rotorcraft Forum*, Hamburg, Germany, Sept. 22–25 2009.

[18] Jeong, J., and Hassan, F., "On the Identification of a Vortex," *Journal of Fluid Mechanics*, Vol. 285, 1995, pp. 69–94.
doi:10.1017/S0022112095000462

[19] Ong, L., and Wallace, J., "The Velocity Field of the Turbulent Very Near Wake of a Circular Cylinder," *Experiments in Fluids*, Vol. 20, No. 6, 1996, pp. 441–453.

[20] Son, J., and Hanratty, T. J., "Velocity Gradients at the Wall for Flow Around a Cylinder at Reynolds Numbers 5×10^3 to 10^5," *Journal of Fluid Mechanics*, Vol. 35, No. 2, 1969, pp. 353–368.
doi:10.1017/S0022112069001157

[21] Kravchenko, A. G., and Moin, P., "Numerical Studies of Flow over a Circular Cylinder at $Re_D = 3900$," *Physics of Fluids*, Vol. 12, No. 2, 2000, pp. 403–417.
doi:10.1063/1.870318

P. Tucker
Associate Editor